JACS
JOURNAL OF THE AMERICAN CHEMICAL SOCIETY
pubs.acs.org/JACS
Article

Two-Dimensional Pb Square Nets from Bulk $(RO)_nPb$ (R = Rare Earth Metals, n = 1,2)

Xu Chen,[#] Jun Deng,[#] Shifeng Jin,[#] Tianping Ying,[*] Ge Fei, Huifen Ren, Yunfan Yang, Ke Ma, Mingzhang Yang, Junjie Wang, Yanchun Li, Xin Chen, Xiaobing Liu, Shixuan Du,[*] Jian-gang Guo,[*] and Xiaolong Chen[*]

Cite This: *J. Am. Chem. Soc.* 2023, 145, 17435−17442

ABSTRACT: All two-dimensional (2D) materials of group IV elements from Si to Pb are stabilized by carrier doping and interface bonding from substrates except graphene which can be free-standing. The involvement of strong hybrid of bonds, adsorption of exotic atomic species, and the high concentration of crystalline defects are often unavoidable, complicating the measurement of the intrinsic properties. In this work, we report the discovery of seven kinds of hitherto unreported bulk compounds $(RO)_nPb$ (R = rare earth metals, n = 1,2), which consist of quasi-2D Pb square nets that are spatially and electronically detached from the $[RO]^{\delta+}$ blocking layers. The band structures of these compounds near Fermi levels are relatively clean and dominantly contributed by Pb, resembling the electron-doped free-standing Pb monolayer. The R_2O_2Pb compounds are metallic at ambient pressure and become superconductors under high pressures with much enhanced critical fields. In particular, Gd_2O_2Pb (9.1 μ_B/Gd) exhibits an interesting bulk response of lattice distortion in conjunction with the emergence of superconductivity and magnetic anomalies at a critical pressure of 10 GPa. Our findings reveal the unexpected facets of 2D Pb sheets that are considerably different from their bulk counterparts and provide an alternative route for exploring 2D properties in bulk materials.

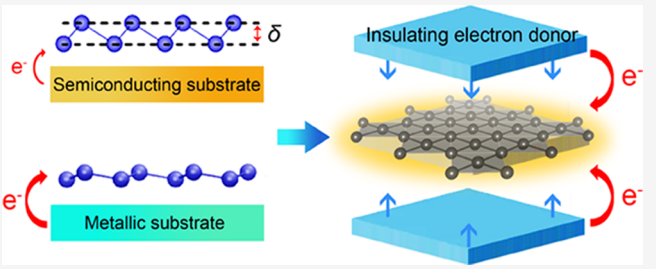

INTRODUCTION

Since the discovery of graphene, the isolation of materials down to atomic thickness reveals exotic properties and attracts continuing enthusiasm. This is typically achieved through either mechanical exfoliation or atomic epitaxy, known as top-down or bottom-up strategies, respectively.[1,2] Thus far, only carbon in group IV elements (C to Pb) can be prepared as free-standing graphene through exfoliation. All other 2D monoelements in this group have to be grown on specific substrates using molecular-beam epitaxy.[3−10] The synergy of hybrid bonding and carrier donation from the substrates plays a crucial role in stabilizing the 2D structures, which would otherwise form clusters.[11,12] However, due to the strong bonding at the interface, the electron and phonon bands of the substrates will intermingle with those of the monolayers.[13,14] The adsorption of exotic atomic species and the presence of unavoidable defects in these artificial structures will further complicate the characterization of their intrinsic properties. It is therefore highly desired to pursue another route to avoid the influence of the substrate, preferably realizing the 2D electronic bands in a bulk material.

Such an idea has recently been proposed in a bulk superlattice $Ba_6Nb_{11}S_{28}$, which consists of a superconducting 2*H*-NbS_2 layer and a commensurate block layer.[15] The presence of sandwiched insulating layers significantly reduces the dimensionality of the bulk material, allowing it to behave as a clean, 2D superconductor with high carrier mobility and vanishing interlayer band dispersion. Similar 2D band structures are also found in layered materials such as La_2CuO_4 and LaOFeAs,[16,17] in which the bands of the insulating $(La_2O_2)^{2+}$ layer do not hybridize with those of the conducting layer, resulting in a cylinder-like Fermi surface. Nevertheless, despite the large number of layered group IV compounds available in databases, such as PbFCl- and $ThCr_2Si_2$-type structures, they cannot be considered as 2D monoelements due to the presence of strong bonds like Pb-Cl, Pb-F, and Si-Cr. Given these observations, a promising approach may be designing a new type of layered structure with alternating insulating layers, such as the $[La_2O_2]^{2+}$ block, and planar 2D monoelement layers, which means that prominent electrons will be simultaneously doped into the group IV elements.

Received: June 11, 2023
Published: July 31, 2023

https://doi.org/10.1021/jacs.3c05807
J. Am. Chem. Soc. 2023, 145, 17435−17442

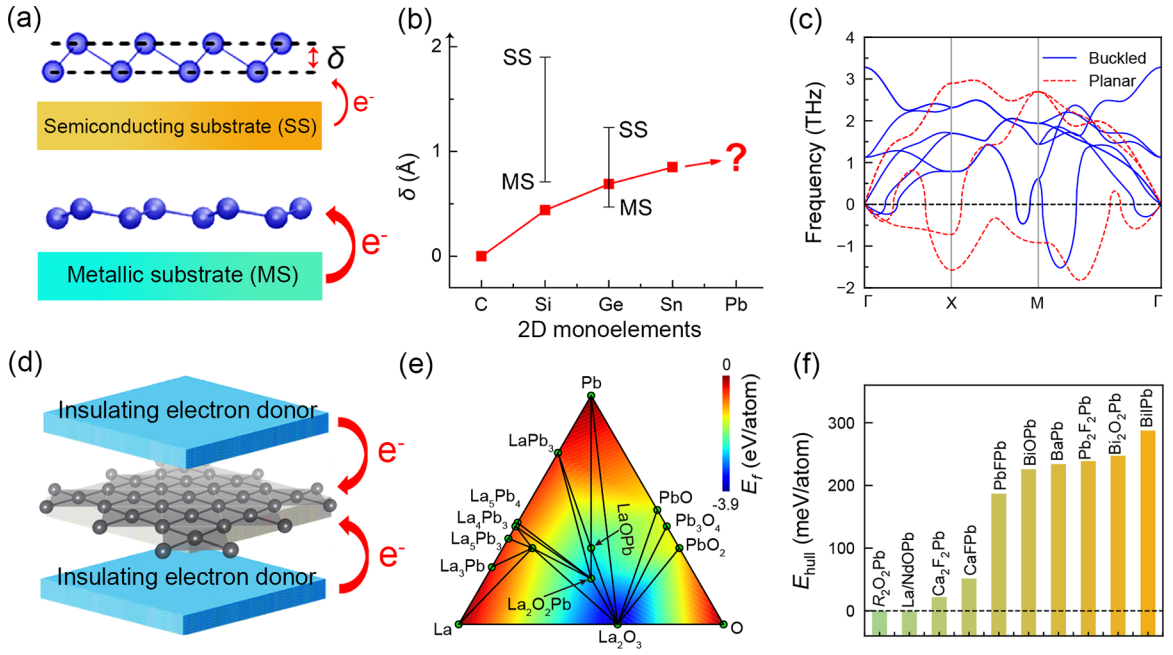

Figure 1. Charge-morphology relationship of 2D monoelements and theoretical design of 2D-Pb square nets. (a) Schematic illustration of the vertical buckling height δ of 2D monoelements grown on different substrates with varying charge transfer abilities. SS and MS are shorthand notations for semiconducting and metallic substrates, respectively. (b) Theoretically predicted δ of group-IV 2D monoelements.[3] The vertical bars represent the experimental range of δ for silicene and germanene grown on various substrates.[3,18−21] (c) Phonon dispersion of free-standing buckled and planar Pb monolayer, which shows large negative frequencies. (d) Schematic diagram of charge transfer from the insulating layer to the Pb layer. (e) Phase diagram of the La−O−Pb system. The color shows the magnitude of the enthalpies (E_f). The predicted La_2O_2Pb and LaOPb are exactly on the convex hull. (f) Energy above hull (E_{hull}) for designed structures, where E_{hull} = 0 eV/atom, indicates that it is stable in energy. "R" refers to Y, La, Sm, Gd, and Er.

Interestingly, excess electron doping should, in principle, facilitate the formation of 2D-monoelement layers. As shown in Figure 1a,b, the vertical buckling height (δ) in 2D monoelements is determined by the ratio of sp^2 and sp^3 hybridization. With the content of sp^3 increases, the material tends to become more buckled, as is the case with the transition from graphene to stanene.[3] The buckling degree of the Pb monolayer is expected to be particularly high. These monolayers adopt a buckled structure to reduce the formation energy by sharing electrons when the charge transfer from the substrate is insufficient. This is supported by the fact that $\delta_{Si/Ag}$ ($\delta_{Ge/Au}$) = 0.71 (0.47) Å is smaller than δ_{Si/MoS_2} (δ_{Ge/MoS_2}) = 1.90 (0.86) Å, which agrees with the expectation that more electrons should be transferred from the metallic substrate (MS) than the semiconducting substrate (SS).[3,18−21] Therefore, extra electron doping from the insulating layer may serve as a perfect match to stabilize the desired 2D monoelement. In this study, we chose 2D Pb squares as the counter block due to the metallic behavior at high temperatures and superconductivity below 7.19 K in the bulk, as well as its large spin-orbit coupling strength, which may hold promise for exotic physics. It has also been reported that the Pb monolayer grown on the Si(111) substrate shows superconductivity, but the interface phonon mode is found to significantly influence the electron−phonon coupling constant.[22]

By employing the principle of lattice matching and electron doping, we have successfully designed and synthesized seven kinds of layered compounds $(RO)_nPb$ (R = rare earth metals). The Pb square lattices are either planar (n = 2) or buckled (n = 1), depending on the electron charge transfer from their adjacent layers. We verified that planar Pb layers are spatially and electronically detached from their adjacent RO layers and can be considered the "bulk equivalent" of 2D Pb. Additionally, external pressure drives metallic R_2O_2Pb into superconductors. Particularly, Gd_2O_2Pb demonstrates an intriguing lattice distortion at a critical pressure of 10 GPa, which coincides with the emergence of superconductivity and magnetic anomaly. The proposed structure design strategy can also be applied to the formation of monoelement layers for Si, Ge, Sn, and even their nearby elements in group III and group V. The $(La_2O_2)^{2+}$ layer can also be replaced by other alternatives. A wide swath of unexplored material realm is waiting to be discovered.

EXPERIMENTAL SECTION

Synthesis. Polycrystalline samples of $(RO)_nPb$ (R = rare earth metals, n = 1,2) were synthesized by conventional solid-state reaction. The powders of R_2O_3, R, and Pb were weighted as the stoichiometric ratio, thoroughly ground, and pelleted under a pressure of 50 MPa in an argon-filled glove box. The pellet was loaded into an Al_2O_3 crucible and sealed into an evacuated silica tube, which was heated up to 1270 K and kept at that temperature for 24 h.

Characterization. The powder X-ray diffraction (PXRD) pattern of the obtained sample was collected at room temperature using a Panalytical diffractometer with Cu K_α (λ = 1.5408 Å) radiation. Rietveld refinement of the PXRD patterns was performed using Fullprof software suites.[23] The resistivity (R) and dc magnetic susceptibility (χ) were measured using the physical property measurement system (PPMS, Quantum Design). The Hall signal was acquired using an AC resistance bridge setup.

In-Situ High-Pressure Measurements. In-situ high-pressure electrical transport of Gd_2O_2Pb, La_2O_2Pb, Er_2O_2Pb, and LaOPb

https://doi.org/10.1021/jacs.3c05807
J. Am. Chem. Soc. 2023, 145, 17435−17442

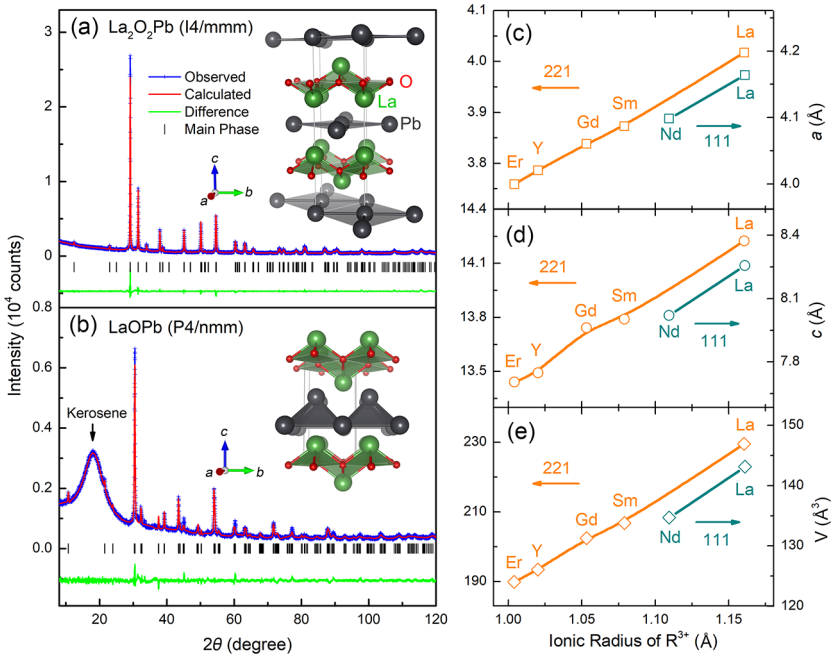

Figure 2. Crystal structures of $(RO)_nPb$. (a) and (b) X-ray diffraction patterns and Rietveld refinements of La_2O_2Pb and LaOPb, respectively, with insets displaying their crystal structures. (c–e) Evolution of lattice parameters for both layered structures as the ionic radius varies.

polycrystalline samples were measured in a physical property measurement system (PPMS, Quantum Design). In-situ high-pressure experiments were conducted using a diamond anvil cell (DAC) with a culet diameter of 300 μm. The electrical transport properties were measured using the four-wire method. To apply pressure, cubic boron nitride (cBN) powders were utilized as both the pressure medium and insulating material. The R_2O_2Pb sample, with dimensions of approximately 100 μm × 100 μm × 10 μm, was carefully positioned within the boron nitride hole. Four platinum (Pt) wires, each with a diameter of 20 μm, were then attached to the surface of the sample. The pressure was measured using the ruby fluorescence method at room temperature each time before and after the measurement. In situ high-P synchrotron powder XRD experiments were performed at the 4W2 station of the Beijing Synchrotron Radiation Facility (BSRF) with a wavelength of 0.6199 Å (20 keV) and a spot size of 35 μm × 12 μm. Silicone oil was used as the pressure-transmitting medium in synchrotron measurements, and the pressure was applied through a continuous pneumatic pressurization system.

Theoretical Calculations. First-principles calculations were performed with the Vienna ab-initio simulation package (VASP).[24] We adopted the generalized gradient approximation (GGA) in the form of the Perdew–Burke–Ernzerhof (PBE)[25] for the exchange-correlation potentials. The projector augmented-wave (PAW) pseudopotentials were used with a plane wave energy 440 eV. $5s^25p^65d^16s^2$, $2s^22p^4$, and $6p^26s^2$ electron configurations were treated as valence electrons for La, O, and Pb, respectively. A Monkhost–Pack[26] Brillouin zone sampling grid with a resolution of $0.02 \times 2\pi$ Å^{-1} was applied. Atomic positions and lattice parameters were relaxed until all the forces on the ions were less than 10^{-2} eV/Å. The Fermi surface was visualized by the Fermisurfer package.[27]

RESULTS AND DISCUSSION

We first check the phonon dispersion of the free-standing 2D Pb lattices with either planar or buckled geometry shown in Figure 1c. The large negative frequencies indicate that the detached Pb planes cannot survive on their own. According to the gradual increase in interatomic distances from C–C of 1.42 Å to Sn-Sn of 2.83 Å, the Pb–Pb distance should be larger than 3.1 Å. Therefore, by setting the Pb–Pb distance at 3.1–4.1 Å and utilizing $[La_2O_2]^{2+}$ as a charge compensator (Figure 1d), we constructed two types of layered structures: LaOPb with a buckled Pb layer and La_2O_2Pb with planar ones. Both lattices are commensurate stacking of $[La_2O_2]^{2+}$ and Pb layers, while the buckled one can be considered as a $\sqrt{2} \times \sqrt{2}$ superstructure of the planar one. Figure 1e shows the ternary phase diagram of La–O–Pb, which is obtained by a convex hull analysis of their formation enthalpies (details can be found in the Supporting Information). Both LaOPb and La_2O_2Pb lie on the convex hull in the phase diagram, demonstrating their thermodynamical stability. Moreover, our phonon calculations show no imaginary frequencies, indicating the lattice-dynamic stability of these layered structures (Figure S1).

Buoyed by the results above, we build a workflow to search other bulk structures consisting of Pb square lattice and ionic insulating layers. By utilizing the in-house-charged building block database,[28] we first look for insulating layers with a lattice mismatch less than 5%. Then, we assemble them with planar/buckled Pb monolayer to form a layered structure, which yields 15 candidates. The corresponding configurations are shown in Figure S2. Finally, their thermodynamic stabilities are estimated by convex hull analysis of their formation enthalpies. We find that the lanthanide oxides are energetically stable with E_{hull} = 0 meV/atom, as summarized in Figure 1f.

Next, we used the conventional solid-state method to synthesize five types of R_2O_2Pb (R = Y, La, Sm, Gd, and Er), representing a range of rare earth elements of different sizes, and two types of $ROPb$ (R = La and Nd) as a proof of the concept. The XRD pattern and crystal structure of La_2O_2Pb are depicted in Figure 2a, and the diffractions of other materials are included in the Supporting Information Figure S3. Table S1 summarizes the Rietveld refinement results, which show that Pb occupies the Wyckoff position 2a in all cases, resulting in a planar Pb square. In contrast, the LaOPb material exhibits a buckled Pb structure (Figure 2b) due to insufficient charge transfer from the adjacent $[La_2O_2]^{2+}$ layer, as discussed in the Introduction. The evolution of the lattice parameters for both systems with the variation of cation radius

https://doi.org/10.1021/jacs.3c05807
J. Am. Chem. Soc. 2023, 145, 17435–17442

is summarized in Figure 2c–e, following the canonical Vegard's law.

While the choice of lanthanide in R_2O_2Pb covers the entire range of rare earth elements, we find that *R*OPb can only be acquired for lanthanides with large atomic radii, from La to Nd. Our attempts to synthesize SmOPb only resulted in a mixture of Sm_2O_2Pb and Pb. This can be explained by the fact that electron doping of a layered material will expand its *ab*-plane and shrink the *c*-axis.[29,30] As shown in Figure 2c, the predicted value of the *a*-axis for SmOPb is 4.05 Å, which is too narrow to accommodate the buckled Pb layer (*R*OPb can be viewed as a $\sqrt{2} \times \sqrt{2}$ reconstruction of R_2O_2Pb), but falls within the range of R_2O_2Pb (3.75 Å < *a* < 4.05 Å) for the formation of a planar Pb lattice. The phase transformation of *R*OPb to R_2O_2Pb for small rare earth elements is therefore driven by the synergistic effect of charge transfer and lattice mismatch.

After confirming the existence of R_2O_2Pb and *R*OPb in the experiment, we resort to density functional theory (DFT) functional calculations to clarify the 2D nature of electronic structures. Here, we take La_2O_2Pb as an example for it contains no *f* valence electrons. Figure 3a shows the Fermi surface of

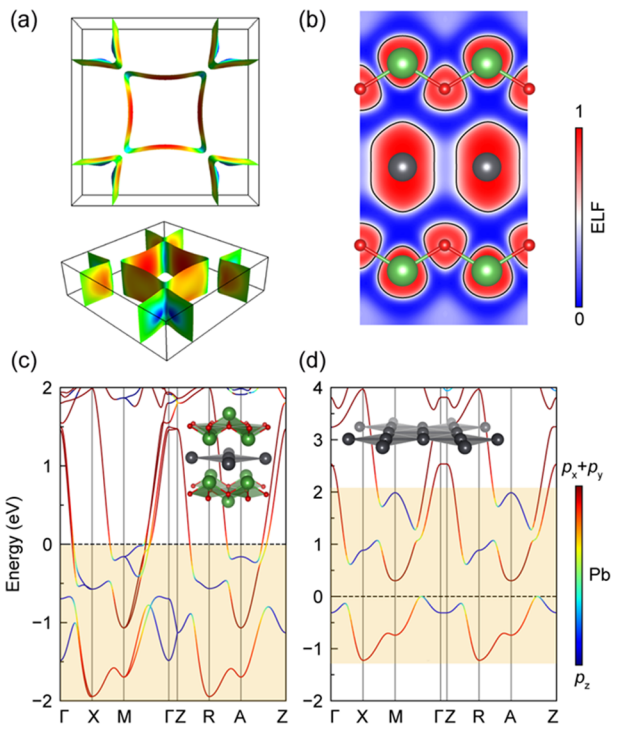

Figure 3. 2D nature in the electronic structure of La_2O_2Pb. (a) Fermi surface of top (up panel) and side (bottom panel) view, (b) (020) slice of electron localization function (ELF) and (c) band structure for La_2O_2Pb. (d) Band structure of Pb monolayers, which is obtained by merely removing $[La_2O_2]^{2-}$ layers in La_2O_2Pb. The colors in the band structures indicate the contribution from $p_x + p_y$ and p_z of Pb, and the yellow shadow shows the comparable region between the two bands. The spin-orbit coupling (SOC) is included in these calculations.

La_2O_2Pb. It is composed of two quasi-square columns around Γ and *M* with low dispersion along the *z* direction, implying a two-dimensional electronic behavior in the *xy* plane. Our density of states calculation shows that Pb-*p* states contribute most around the Fermi level (Figure S4). Besides, the electron localization function (ELF) shows that there is no obvious covalent bonding between Pb and $[La_2O_2]^{2-}$ layers, referring to ionic bonding between them in nature (Figure 3b). This confirms that the 2D Pb is spatially detached from its adjacent $(La_2O_2)^{2+}$ layers. To further reveal the influence of $[La_2O_2]^{2-}$ layers on the electronic structures, we calculated the electronic structure (Figure 3d) of Pb monolayers by simply removing $[La_2O_2]^{2-}$ layers. Compared with the band structure of La_2O_2Pb shown in Figure 3c, we find that the bands contributed by Pb layers are almost unchanged, despite the energy shift due to charge doping and band degeneration at several *K* points because of the high symmetry. The independent feature of the band structure proves that $[La_2O_2]^{2+}$ serves as an electron compensator. Moreover, the states of Pb-p_z have lower dispersion than those of Pb-p_x/p_y, because of its weak interaction with $[La_2O_2]^{2+}$ layer along the *z* direction. A similar phenomenon occurs in LaOPb, where buckled Pb layer determines the whole electronic property of the system, and $[La_2O_2]^{2+}$ provides carriers (Figure S5). These results indicate that the Pb square lattice almost keeps the 2D character as in the monolayer form.

Having established the electronic 2D nature in these bulk materials, we further investigated the transport properties of the planar and buckled Pb squares. Both families of materials, R_2O_2Pb and *R*OPb, are metals at ambient pressure (as shown in Figure S6). The Hall measurements of Gd_2O_2Pb show a hole carrier concentration of approximately 1×10^{22} cm^{-3} in the entire temperature range (Figure S7), which is much smaller than that of bulk Pb (5×10^{23} cm^{-3})[31] and in line with the hole pocket at the Γ point seen in Figure 3c.

Under external pressure, we find that R_2O_2Pb compounds are successfully driven into superconductors; meanwhile, no evidence of superconductivity is observed in the *R*OPb series synthesized and pressed using the same procedure. The observed superconductivity cannot be attributed to trace impurities such as Pb that are beyond the detection limit of X-ray diffraction. This is because the T_c of Pb would quickly get suppressed from its ambient pressure value of 7.2–2.4 K at 12 GPa.[32] We also noticed that large excitation currents can result in residual resistance (Figure S8), but it does not have a significant influence on the onset transition temperature. While La_2O_2Pb exhibits a higher T_c of 6.9 K (Figure S9), we performed a detailed investigation on Gd_2O_2Pb because Gd has an unsaturated magnetic moment of 9.1 μ_B/Gd and antiferromagnetic (AFM) transition temperature T_N of 12 K, as shown in Figure 4a.

We proceed to investigate the structural evolution of Gd_2O_2Pb up to 25 GPa using synchrotron diffractions. Figure 4b depicts the evolution of low-angle diffraction peaks, specifically 103 and 110, as the external pressure is varied. The corresponding raw data and full-range contour plot can be found in Figure S10. The red and cyan lines in Figure 4b serve as visual guides, from which we have two intriguing discoveries. First, distinct noncontinuous kinks are observed at around 10 GPa, resulting in changes in slope for both peaks. Second, there is an abrupt change in peak intensity, indicated by the coloration in Figure 4b. Figure 4c presents a summary of the pressure-dependent lattice constants for the *a* and *c* axes, confirming the results observed in Figure 4b. While the Gd_2O_2Pb compound maintains the *I*4/mmm space group above and below the critical pressure, notable changes in lattice parameters suggest a first-order phase transition. Specifically, the *c*-axis contracts while the *a*-axis elongates at 10 GPa.

https://doi.org/10.1021/jacs.3c05807
J. Am. Chem. Soc. 2023, 145, 17435–17442

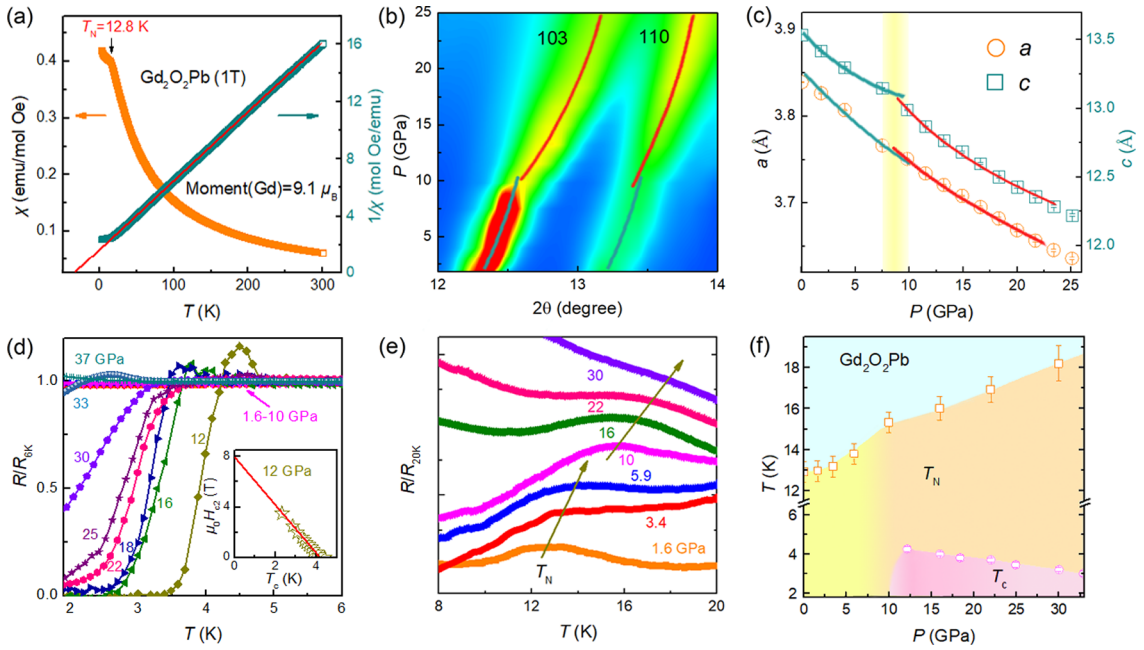

Figure 4. Lattice distortion, magnetic anomaly, and superconductivity in pressurized Gd_2O_2Pb. (a) Temperature-dependent magnetic susceptibility and the fitting results of Gd_2O_2Pb at ambient pressure. (b) Color contour of the synchrotron diffractions 103 and 110 with varying external pressure. The full angle plot and their raw data can be found in Figure S9. (c) Extracted lattice constant of *a* and *c* axes with the variation of external pressure. (d) Normalized resistance of Gd_2O_2Pb as a function of applied external pressure. Inset shows the extrapolation of the upper critical field to zero temperature, resulting in an H_{c2} of 8 T. (e) Normalized resistivity of Gd_2O_2Pb with the applied external pressure in the temperature range 8−20 K. (f) Phase diagram of Gd_2O_2Pb.

Table 1. Crystallographic Parameters and Properties of $(RO)_nPb$

	R_2O_2Pb (*I*4/*mmm*)					ROPb (*P*4/*nmm*)	
R	La	Sm	Gd	Y	Er	La	Nd
a (Å)	4.0176 (1)	3.8727 (2)	3.8384 (1)	3.7862 (1)	3.7588 (1)	4.1639 (1)	4.0983 (4)
c (Å)	14.2248 (4)	13.7910 (8)	13.7420 (6)	13.4932 (4)	13.4422 (5)	8.2565 (3)	8.0198 (9)
V (Å^3)	229.60 (2)	206.84 (3)	202.47 (2)	193.43 (1)	189.91 (1)	143.15 (1)	134.71 (3)
Pb−Pb(Å)	4.0176 (1)	3.8727 (2)	3.8384 (1)	3.7862 (1)	3.7588 (1)	3.718 (3)	3.636 (3)
Ambient*	M	M	M (AFM)	M	M	M	M
high *P*	SC (6.9 K)		AFM + SC (4.5 K)		SC (3.6 K)	M	
H_{c2}^0	8.8 T		8.0 T		5.8 T		

This structural change coincides with the emergence of superconductivity. Figure 4d illustrates a superconducting transition at 12 GPa, with the highest onset T_c reaching 4.8 K. The typical *I*−*V* curve of Gd_2O_2Pb at 1.8 K can be found in Figure S11, confirming the emergence of superconductivity. Below 10 GPa, no signs of superconductivity are observed. This behavior is reminiscent of the phenomenon of interlayer collapsing-induced superconductivity observed in materials such as $FePSe_3$.[33,34] Additionally, T_c is gradually suppressed by an external field (Figure S12) with a linearly extrapolated upper critical magnetic field (H_{c2}^0) of 8 T, which is two orders of magnitude higher than that of bulk Pb. The linear H_{c2}−T_c relationship (inset of Figure 4d) has also been observed in other 2D superconductors.[33,35] At a moderate temperature range, the resistivity shows a kink at 12 K, which is due to reduced electron scattering and coincides with the AFM transition. We therefore traced this kink under various external pressures (Figure 4e). By summarizing all the data in Figure 4f, we observed an intriguing anomalous hump in the T_N at around 10 GPa. An intuitive explanation for this phenomenon lies in the reinforcement of interlayer interactions, which promotes antiferromagnetism and triggers the onset of superconductivity.

Superconductivity has previously been reported in a Pb monolayer grown on the Si(111) substrate, with its T_c increasing as the atom areal density of Pb increases.[22] The T_cs of the Pb monolayer is found to be 1.83 and 1.52 K for Pb densities of 10.44 and 9.40 Pb atoms nm^{-2}, respectively.[22] Linearly extrapolating these results, we estimate that the T_c of our La_2O_2Pb sample at ambient pressure would be 0.57 K using the lattice parameter a^2 of the squared Pb lattice (0.16 nm^2 per Pb, namely, 6.25 Pb atoms nm^{-2}). Note that this is a rough estimate and does not take into account the significant contribution of the substrate phonons of Si(111) to the electron−phonon coupling in the Pb monolayer.[22] It is recently discovered that the isolated CuO_2 plane from $Bi_2Sr_2CaCu_2O_{8+\delta}$, segregated by the insulating $Bi_4Sr_4Ca_2O_8$ layer, shows almost identical superconductivity to its bulk form.[36,37] Measurements down to ultra-low temperature may reveal more characteristics of their ground states at ambient pressure. Nevertheless, the emergence of T_c at high pressure with a much-enhanced H_{c2} is distinct from their 3D-Pb

https://doi.org/10.1021/jacs.3c05807
J. Am. Chem. Soc. 2023, 145, 17435−17442

counterpart, suggesting a different pairing mechanism in the reduced dimensionality.

It is uncommon for superconductivity to coexist with magnetic ordering,[38−41] as superconductivity typically emerges when the AFM is completely suppressed. The current understanding of the evolution of superconductivity and magnetization under external pressure is primarily based on electrical transport measurements, while the characterization through pressure magnetometry is lacking. Further investigations are highly desired to elucidate the bulk signal of superconductivity and unravel the intricate interplay with magnetization. From Figure 4f, it is evident that the T_c exhibits an opposite trend to the increasing T_N, indicating a competition between superconductivity and magnetic ordering in Gd_2O_2Pb. This coexistence and competition between superconductivity and magnetic ordering, though uncommon, have been reported in several other layered superconductors such as $RbEuFe_4As_4$,[42] $Eu_{0.5}Ce_{0.5}BiS_2F$,[43] and $Nd_{1.85}Ce_{0.15}CuO_4$.[44] In these materials, the magnetic layers are spatially separated from the superconducting layers, similar to the case of Gd_2O_2Pb. Further experimental investigations and theoretical calculations are highly warranted to delve into this captivating coexistence regime.

The compounds synthesized in this work are summarized in Table 1, representing only a small portion of the potential candidates of monolayers sandwiched between insulating layers. At the outset, it is worth noting that the synthesis of other two-dimensional monoelements, such as Si, Ge, and Sn, as well as other *p*-block elements or even *d*-block metals, is possible using the method described here,[3−10,45−48] and has the potential to yield a wide range of new material categories with unique properties. By carefully controlling the charge donation from the $[La_2O_2]^{2+}$ layer through the substitution of divalent alkali-earth elements, it is possible to precisely adjust the buckling height and thereby alter the transport properties of the underlying 2D-Pb square net. It is worth noting that the mere stacking of two separate sublattices, with one being conducting and the other being insulating, does not guarantee the formation of a perfect 2D Fermi surface. This can be exemplified by the well-known compound LaOFeAs, where the presence of band dispersion along the *z* direction is clearly observed.[17,49] The design of heterostructures with alternating planar and buckled two-dimensional layers is also a promising direction for future research. The next challenge is to grow single crystals of these layered structures, which would allow for the study of their anisotropic transport properties, carrier mobility, and various spectroscopy measurements.

CONCLUSIONS

In conclusion, we report the design and discovery of seven new kinds of layered structures consisting of alternating layers of 2D Pb and insulating blocks. These materials stand out from other layered compounds by their planar or buckled square Pb nets, which are spatially and electronically separate from each other. The prominent charge transfer from its adjacent rare-earth oxide layers plays a vital role in stabilizing the sandwiched Pb layers and dictating the morphology of the 2D structures. The realization of superconductivity in the layered R_2O_2Pb family and its coexistence with magnetic ordering highlight the uniqueness of synthesized compounds, which provide an alternative route to explore the fairyland of 2D phenomena.

ASSOCIATED CONTENT

Supporting Information

The Supporting Information is available free of charge at https://pubs.acs.org/doi/10.1021/jacs.3c05807.

Detailed experimental procedures; computational details; powder diffractions of the remaining (RO)nPb; Rietveld refinement results; band structures of LaOPb; and transport properties and synchrotron diffractions (PDF)

AUTHOR INFORMATION

Corresponding Authors

Tianping Ying − *Beijing National Laboratory for Condensed Matter Physics, Institute of Physics, Chinese Academy of Sciences, Beijing 100190, China;* orcid.org/0000-0001-7665-1270; Email: ying@iphy.ac.cn

Shixuan Du − *Beijing National Laboratory for Condensed Matter Physics, Institute of Physics, Chinese Academy of Sciences, Beijing 100190, China;* orcid.org/0000-0001-9323-1307; Email: sxdu@iphy.ac.cn

Jian-gang Guo − *Beijing National Laboratory for Condensed Matter Physics, Institute of Physics, Chinese Academy of Sciences, Beijing 100190, China; Songshan Lake Materials Laboratory, Dongguan, Guangdong 523808, China;* orcid.org/0000-0003-3880-3012; Email: jgguo@iphy.ac.cn

Xiaolong Chen − *Beijing National Laboratory for Condensed Matter Physics, Institute of Physics, Chinese Academy of Sciences, Beijing 100190, China; School of Physical Sciences, University of Chinese Academy of Sciences, Beijing 100049, China; Songshan Lake Materials Laboratory, Dongguan, Guangdong 523808, China;* orcid.org/0000-0001-8455-2117; Email: chenx29@iphy.ac.cn

Authors

Xu Chen − *Beijing National Laboratory for Condensed Matter Physics, Institute of Physics, Chinese Academy of Sciences, Beijing 100190, China;* orcid.org/0000-0003-3477-2204

Jun Deng − *Beijing National Laboratory for Condensed Matter Physics, Institute of Physics, Chinese Academy of Sciences, Beijing 100190, China;* orcid.org/0000-0003-2420-8079

Shifeng Jin − *Beijing National Laboratory for Condensed Matter Physics, Institute of Physics, Chinese Academy of Sciences, Beijing 100190, China*

Ge Fei − *Laboratory of High Pressure Physics and Material Science (HPPMS), School of Physics and Physical Engineering, Qufu Normal University, Qufu 273100, China*

Huifen Ren − *Beijing National Laboratory for Condensed Matter Physics, Institute of Physics, Chinese Academy of Sciences, Beijing 100190, China*

Yunfan Yang − *Beijing National Laboratory for Condensed Matter Physics, Institute of Physics, Chinese Academy of Sciences, Beijing 100190, China; School of Physical Sciences, University of Chinese Academy of Sciences, Beijing 100049, China*

Ke Ma − *Beijing National Laboratory for Condensed Matter Physics, Institute of Physics, Chinese Academy of Sciences, Beijing 100190, China; School of Physical Sciences, University of Chinese Academy of Sciences, Beijing 100049, China*

Mingzhang Yang − *Beijing National Laboratory for Condensed Matter Physics, Institute of Physics, Chinese Academy of Sciences, Beijing 100190, China; School of Physical Sciences, University of Chinese Academy of Sciences, Beijing 100049, China*

Junjie Wang − *Beijing National Laboratory for Condensed Matter Physics, Institute of Physics, Chinese Academy of Sciences, Beijing 100190, China; School of Physical Sciences, University of Chinese Academy of Sciences, Beijing 100049, China*

Yanchun Li − *Beijing Synchrotron Radiation Facility Institute of High Energy Physics, Chinese Academy of Sciences, Beijing 100049, China*

Xin Chen − *Laboratory of High Pressure Physics and Material Science (HPPMS), School of Physics and Physical Engineering, Qufu Normal University, Qufu 273100, China;* orcid.org/0000-0003-0652-0798

Xiaobing Liu − *Laboratory of High Pressure Physics and Material Science (HPPMS), School of Physics and Physical Engineering, Qufu Normal University, Qufu 273100, China;* orcid.org/0000-0002-0680-1947

Complete contact information is available at: https://pubs.acs.org/10.1021/jacs.3c05807

Author Contributions

[#]X.C., J.D., and S.F.J. contributed equally to this work.

Notes

The authors declare no competing financial interest.

■ ACKNOWLEDGMENTS

We gratefully acknowledge Dr. J. Guo and Dr. P.T. Yang for measuring physical properties. This work is financially supported by the National Key Research and Development Program of China (no. 2021YFA1401800), Beijing Natural Science Foundation (grant no. Z200005), the National Natural Science Foundation of China (nos. 52272267, 52250308, 52202342, 51922105, 61888102, and 62022089), the Shandong Provincial Natural Science Foundation (ZR2020YQ05, ZR2019MA054, and 2019KJJ020), the Youth Innovation Promotion Association of CAS (grant no. 2019005), and the Synergetic Extreme Condition User Facility (SECUF). ADXRD measurements were performed at 4W2 High Pressure Station, Beijing Synchrotron Radiation Facility (BSRF), which is supported by the Chinese Academy of Sciences (grant KJCX2-SW-N20 and KJCX2-SW-N03).

■ REFERENCES

(1) Geim, A. K.; Novoselov, K. S. The rise of graphene. *Nat. Mater.* **2007**, *6*, 183.

(2) Geim, A. K.; Grigorieva, I. V. Van der Waals heterostructures. *Nature* **2013**, *499*, 419.

(3) Molle, A.; Goldberger, J.; Houssa, M.; Xu, Y.; Zhang, S. C.; Akinwande, D. Buckled two-dimensional Xene sheets. *Nat. Mater.* **2017**, *16*, 163.

(4) Duong, D. L.; Yun, S. J.; Lee, Y. H. van der Waals layered materials: opportunities and challenges. *ACS Nano* **2017**, *11*, 11803.

(5) Mannix, A. J.; Kiraly, B.; Hersam, M. C.; Guisinger, N. P. Synthesis and chemistry of elemental 2D materials. *Nat. Rev. Chem.* **2017**, *1*, No. 0014.

(6) Yuhara, J.; He, B.; Matsunami, N.; Nakatake, M.; le Lay, G. Graphene's latest cousin: plumbene epitaxial growth on a "Nano WaterCube". *Adv. Mater.* **2019**, *31*, No. 1901017.

(7) Meng, L.; Wang, Y.; Zhang, L.; Du, S.; Wu, R.; Li, L.; Zhang, Y.; Li, G.; Zhou, H.; Hofer, W. A.; Gao, H. J. Buckled silicene formation on Ir(111). *Nano Lett.* **2023**, *13*, 685.

(8) Li, L.; Lu, S. Z.; Pan, J.; Qin, Z.; Wang, Y. Q.; Wang, Y.; Cao, G. Y.; du, S.; Gao, H. J. Buckled germanene formation on Pt(111). *Adv. Mater.* **2014**, *26*, 4820.

(9) Qin, Z.; Pan, J.; Lu, S.; Shao, Y.; Wang, Y.; du, S.; Gao, H. J.; Cao, G. Buckled direct evidence of Dirac signature in bilayer germanene islands on Cu(111). *Adv. Mater.* **2017**, *29*, No. 1606046.

(10) Huang, L.; Zhang, Y. F.; Zhang, Y. Y.; Xu, W.; Que, Y.; Li, E.; Pan, J. B.; Wang, Y. L.; Liu, Y.; du, S. X.; Pantelides, S. T.; Gao, H. J. Sequence of silicon monolayer structures grown on a Ru surface: from a herringbone structure to silicene. *Nano Lett.* **2017**, *17*, 1161.

(11) Tao, L.; Cinquanta, E.; Chiappe, D.; Grazianetti, C.; Fanciulli, M.; Dubey, M.; Molle, A.; Akinwande, D. Silicenefield-effect transistors operatingat room temperature. *Nature* **2015**, *10*, 227.

(12) Bihlmayer, G.; Sassmannshausen, J.; Kubetzka, A.; Blügel, S.; von Bergmann, K.; Wiesendanger, R. Plumbene on a magnetic substrate: a combined scanning tunneling microscopy and density functional theory study. *Phys. Rev. Lett.* **2020**, *124*, No. 126401.

(13) Giovannetti, G.; Khomyakov, P. A.; Brocks, G.; Karpan, V. M.; van den Brink, J.; Kelly, P. J. Doping graphene with metal contacts. *Phys. Rev. Lett.* **2008**, *101*, No. 026803.

(14) Gao, Y. X.; Zhang, Y. Y.; du, S. Recovery of the Dirac states of graphene by intercalating twodimensional traditional semiconductors. *J. Phys.: Condens. Matter* **2019**, *31*, 194001.

(15) Devarakonda, A.; Inoue, H.; Fang, S.; Ozsoy-Keskinbora, C.; Suzuki, T.; Kriener, M.; Fu, L.; Kaxiras, E.; Bell, D. C.; Checkelsky, J. G. Clean 2D superconductivity in a bulk van der Waals superlattice. *Science* **2020**, *370*, 231.

(16) Bednorz, J. G.; Müller, K. A. Possible high T_c superconductivity in the Ba− La− Cu− O system. *Z. Phys. B − Conden. Matter* **1986**, *64*, 189.

(17) Kamihara, Y.; Watanabe, T.; Hirano, M.; Hosono, H. Iron-based layered superconductor La$[O_{1-x}F_x]$FeAs (x = 0.05−0.12) with T_c = 26 K. *J. Am. Chem. Soc.* **2008**, *130*, 3296.

(18) Lin, C. L.; Arafune, R.; Kawahara, K.; Tsukahara, N.; Minamitani, E.; Kim, Y.; Takagi, N.; Kawai, M. Structure of silicene grown on Ag(111). *Appl. Phys. Express* **2012**, *5*, No. 045802.

(19) Chiappe, D.; Scalise, E.; Cinquanta, E.; Grazianetti, C.; van den Broek, B.; Fanciulli, M.; Houssa, M.; Molle, A. Two-dimensional Si nanosheets with local hexagonal structure on a MoS_2 surface. *Adv. Mater.* **2014**, *26*, 2096.

(20) Dávila, M. E.; Xian, L.; Cahangirov, S.; Rubio, A.; Le Lay, G. Germanene: a novel two-dimensional germanium allotrope akin to graphene and silicene. *New J. Phys.* **2014**, *16*, No. 095002.

(21) Zhang, L.; Bampoulis, P.; Rudenko, A. N.; Yao, Q. V.; Van Houselt, A.; Poelsema, B.; Katsnelson, M. I.; Zandvliet, H. J. W. Structural and electronic properties of germanene on MoS_2. *Phys. Rev. Lett.* **2016**, *166*, No. 256804.

(22) Zhang, T.; Cheng, P.; Li, W. J.; Sun, Y. J.; Wang, G.; Zhu, X. G.; He, K.; Wang, L.; Ma, X.; Chen, X.; Wang, Y.; Liu, Y.; Lin, H. Q.; Jia, J. F.; Xue, Q. K. Superconductivity in one-atomic-layer metal films grown on Si(111). *Nat. Phys.* **2010**, *6*, 104.

(23) Rodriguez-carvajal, J. Recent advances in magnetic structure determination neutron powder diffraction. *Physica B* **1993**, *192*, 55.

(24) Kresse, G.; Furthmüller, J. Efficiency of *ab*-initio total energy calculations for metals and semiconductors using a plane-wave basis set. *Comput. Mater. Sci.* **1996**, *6*, 15.

(25) Perdew, J. P.; Burke, K.; Ernzerhof, M. Generalized gradient approximation made simple. *Phys. Rev. Lett.* **1996**, *77*, 3865.

(26) Monkhorst, H. J.; Pack, J. D. Special points for Brillouin-zone integrations. *Phys. Rev. B* **1976**, *13*, 5188.

(27) Kawamura, M. FermiSurfer: Fermi-surface viewer providing multiple representation schemes. *Comput. Phys. Commun.* **2019**, *239*, 197.

(28) Deng, J.; Pan, J.; Zhang, Y. F.; du, S. Database construction of two-dimensional charged building blocks for functional-oriented material design. *Nano Lett.* **2023**, *23*, 4634.

(29) Liu, Y.; Wang, G.; Ying, T.; Lai, X.; Jin, S.; Liu, N.; Hu, J.; Chen, X. Understanding doping, vacancy, lattice stability, and superconductivity in $K_xFe_{2-y}Se_2$. *Adv. Sci.* **2016**, *3*, No. 1600098.
(30) Ying, T. P.; Chen, X.; Wang, G.; Jin, S.; Lai, X.; Zhou, T.; Zhang, H.; Shen, S.; Wang, W. Superconducting phases in potassium-intercalated iron selenides. *J. Am. Chem. Soc.* **2013**, *135*, 2951.
(31) Shiozaki, I.; Sato, T. Effect of temperature on the Hall coefficient of indium and indium-rich solid solutions. *J. Phys. Soc. Jpn.* **1967**, *22*, 105.
(32) Eiling, A.; Schilling, J. S. Pressure and temperature dependence of electrical resistivity of Pb and Sn from 1-300K and 0-10 GPa-use as continuous resistive pressure monitor accurate over wide temperature range; superconductivity under pressure in Pb, Sn and In. *J. Phys. F: Met. Phys.* **1981**, *11*, 623.
(33) Wang, Y.; Ying, J.; Zhou, Z.; Sun, J.; Wen, T.; Zhou, Y.; Li, N.; Zhang, Q.; Han, F.; Xiao, Y.; Chow, P. Emergent superconductivity in an iron-based honeycomb lattice initiated by pressure-driven spin-crossover. *Nat. Commun.* **2018**, *9*, 1914.
(34) Kreyssig, A.; Green, M. A.; Lee, Y.; Samolyuk, G. D.; Zajdel, P.; Lynn, J. W.; Bud'ko, S. L.; Torikachvili, M. S.; Ni, N.; Nandi, S.; Leão, J. B.; Poulton, S. J.; Argyriou, D. N.; Harmon, B. N.; McQueeney, R. J.; Canfield, P. C.; Goldman, A. I. Pressure-induced volume-collapsed tetragonal phase of $CaFe_2As_2$ as seen via neutron scattering. *Phys. Rev. B* **2008**, *78*, No. 184517.
(35) Saito, Y.; Kasahara, Y.; Ye, J.; Iwasa, Y.; Nojima, T. Metallic ground state in an ion-gated two-dimensional superconductor. *Science* **2015**, *350*, 409.
(36) Yu, Y.; Ma, L.; Cai, P.; Zhong, R.; Ye, C.; Shen, J.; Gu, G. D.; Chen, X. H.; Zhang, Y. High-temperature superconductivity in monolayer $Bi_2Sr_2CaCu_2O_{8+\delta}$. *Nature* **2019**, *575*, 156.
(37) Barišić, N.; Chan, M. K.; Li, Y.; Yu, G.; Zhao, X.; Dressel, M.; Smontara, A.; Greven, M. Universal sheet resistance and revised phase diagram of the cuprate high-temperature superconductors. *Proc. Natl. Acad. Sci. U. S. A.* **2013**, *110*, 12235.
(38) Steglich, F.; Aarts, J.; Bredl, C. D.; Lieke, W.; Meschede, D.; Franz, W.; Schäfer, H. Superconductivity in the Presence of Strong Pauli Paramagnetism: $CeCu_2Si_2$. *Phys. Rev. Lett.* **1979**, *43*, 1892.
(39) Stockert, O.; Arndt, J.; Faulhaber, E.; Geibel, C.; Jeevan, H. S.; Kirchner, S.; Loewenhaupt, M.; Schmalzl, K.; Schmidt, W.; Si, Q.; Steglich, F. Magnetically driven superconductivity in $CeCu_2Si_2$. *Nat. Phys.* **2011**, *7*, 119.
(40) Jia, Y. T.; Gong, C. S.; Liu, Y. X.; Zhao, J. F.; Dong, C.; Dai, G. Y.; Li, X. D.; Lei, H. C.; Yu, R. Z.; Zhang, G. M.; Jin, C. Q. Mott transition and superconductivity in quantum spin liquid candidate $NaYbSe_2$. *Chin. Phys. Lett.* **2021**, *37*, No. 097404.
(41) Chen, X.; Zhan, X.; Wang, X.; Deng, J.; Liu, X. B.; Chen, X.; Guo, J. G.; Chen, X. Highly robust reentrant superconductivity in CsV_3Sb_5 under pressure. *Chin. Phys. Lett.* **2021**, *38*, No. 057402.
(42) Collomb, D.; Bending, S. J.; Koshelev, A. E.; Smylie, M. P.; Farrar, L.; Bao, J. K.; Chung, D. Y.; Kanatzidis, M. G.; Kwok, W. K.; Welp, U. Observing the suppression of superconductivity in $RbEuFe_4As_4$ by correlated magnetic fluctuations. *Phys. Rev. Lett.* **2021**, *126*, No. 157001.
(43) Zhai, H. F.; Zhang, P.; Tang, Z. T.; Bao, J. K.; Jiang, H.; Feng, C. M.; Xu, Z. A.; Cao, G. H. Coexistence of superconductivity and complex 4 *f* magnetism in $Eu_{0.5}Ce_{0.5}BiS_2F$. *J. Phys.: Condens. Matter* **2015**, *27*, No. 385701.
(44) Kang, H. J.; Dai, P.; Lynn, J. W.; Matsuura, M.; Thompson, J. R.; Zhang, S. C.; Argyriou, D. N.; Onose, Y.; Tokura, Y. Antiferromagnetic order as the competing ground state in electron-doped $Nd_{1.85}Ce_{0.15}CuO_4$. *Nature* **2003**, *423*, 522.
(45) Mizoguchi, H.; Hosono, H. A metal-insulator transition in R_2O_2Bi with an unusual Bi^{2-} square net (R = rare earth or Y). *J. Am. Chem. Soc.* **2011**, *133*, 2394.
(46) Wang, J.; Ying, T.; Deng, J.; Pei, C.; Yu, T.; Chen, X.; Wan, Y.; Yang, M.; Dai, W.; Yang, D.; Li, Y. Superconductivity in an orbital-reoriented SnAs square lattice: a Case Study of $Li_{0.6}Sn_2As_2$ and NaSnAs. *Angew. Chem., Int. Ed.* **2023**, *62*, No. e202216086.
(47) Feng, B. J.; Li, W. B.; Qiu, J. L.; Cheng, P.; Chen, L.; Wu, K. H. Variable coupling strength of silicene on Ag(111). *Chin. Phys. Lett.* **2015**, *32*, No. 037302.
(48) Wang, P. L.; Kolodiazhnyi, T.; Yao, J.; Mozharivskyj, Y. Decoupling the Electrical Conductivity and Seebeck Coefficient in the RE_2SbO_2 Compounds through Local Structural Perturbations. *J. Am. Chem. Soc.* **2012**, *134*, 1426.
(49) Kuroki, K.; Onari, S.; Arita, R.; Usui, H.; Tanaka, Y.; Kontani, H.; Aoki, H. Unconventional pairing originating from the disconnected Fermi surfaces of superconducting $LaFeAsO_{1-x}F_x$. *Phys. Rev. Lett.* **2008**, *101*, No. 087004.

https://doi.org/10.1021/jacs.3c05807
J. Am. Chem. Soc. 2023, 145, 17435−17442